
CADDA: Class-wise Automatic Differentiable Data Augmentation for EEG Signals

Cédric Rommel

Inria - CEA
Université Paris-Saclay
cedric.rommel@inria.fr

Thomas Moreau

Inria - CEA
Université Paris-Saclay
thomas.moreau@inria.fr

Alexandre Gramfort

Inria - CEA
Université Paris-Saclay
alexandre.gramfort@inria.fr

Abstract

Data augmentation is a key element of deep learning pipelines, as it informs the network during training about transformations of the input data that keep the label unchanged. Manually finding adequate augmentation methods and parameters for a given pipeline is however rapidly cumbersome. In particular, while intuition can guide this decision for images, the design and choice of augmentation policies remains unclear for more complex types of data, such as neuroscience signals. Moreover, label independent strategies might not be suitable for such structured data and class-dependent augmentations might be necessary. This idea has been surprisingly unexplored in the literature, while it is quite intuitive: changing the color of a car image does not change the object class to be predicted, but doing the same to the picture of an orange does. This paper aims to increase the generalization power added through class-wise data augmentation. Yet, as seeking transformations depending on the class largely increases the complexity of the task, using gradient-free optimization techniques as done by most existing automatic approaches becomes intractable for real-world datasets. For this reason we propose to use differentiable data augmentation amenable to gradient-based learning. EEG signals are a perfect example of data for which good augmentation policies are mostly unknown. In this work, we demonstrate the relevance of our approach on the clinically relevant sleep staging classification task, for which we also propose differentiable transformations.

1 Introduction

Data augmentation is a well-known regularization technique, widely used to improve the generalization power of large models, specially in deep learning [1, 2, 3]. Not only does it help by synthetically increasing the size of the dataset used to for training, it also creates useful inductive biases, as it encodes invariances of the data and the underlying decision function which the model does not have to learn from scratch [4, 5]. Such invariant transforms are also a key ingredient for state-of-the-art self-supervised learning [6]. Unfortunately, these transforms have to be known *a priori* and the best augmentations to use often highly depend on the model architecture, the task, the dataset and even the training stage [7, 8]. Manually finding what augmentation to use for a new problem is a cumbersome task, and this motivated the proposal of several automatic data augmentation search algorithms [9].

The existing automatic data augmentation literature often focuses on computer vision problems only, and its application to other scientific domains such as neuroscience has been under-explored. Data augmentation is all the more important in this field, as brain data, be it functional MRI (fMRI) or electroencephalography (EEG) signals, is very scarce either because its acquisition is complicated and costly or because expert knowledge is required for labelling it, or both. Furthermore, while atomic transformations encoding suitable invariances for images are intuitive (if you flip the picture of a cat horizontally it is still a cat), the same cannot be said about magnetic and electrical brain signals. Hence, automatic data augmentation search could be helpful not only to improve the performance of predictive models on EEG data, but also to discover interesting invariances present in brain signals.

Another interesting aspect of data augmentation that has gotten little attention is the fact that suitable invariances often depend on the class considered. When doing object recognition on images, using color transformations during training can help the model to better recognize cars or lamps, which are invariant to it, but will probably hurt the performance for classes which are strongly defined by their color, such as apples or oranges. This also applies to neuroscience tasks, such as sleep staging which is part of a clinical exam conducted to characterize sleep disorders. As most commonly done [10], it consists in assigning to windows of 30 s of signals a label among five: Wake (W), Rapid Eye Movement (REM) and Non-REM of depth 1, 2 or 3 (N1, N2, N3). While some sleep stages are strongly characterized by the presence of waves with a particular shape, such as spindles and K-complexes in the N2 stage, others are defined by the dominating frequencies in the signal, such as alpha and theta rhythms in wake and N1 stages respectively [11]. This means that while randomly setting some small portion of a signal to zero might work to augment W or N1 signals, it might wash out important waves in N2 stages and slow down the learning for this class. This motivates the study of augmentations depending on the class. Of course, as this greatly increases the number of operations and parameters to set, handcrafting such augmentations is not conceivable and efficient automatic searching strategies are required, which is the central topic of this paper. Using black-box optimization algorithms as most automatic data augmentation papers suggest seemed unsuitable given the exponential increase in complexity of the problem when separate augmentations for each class are considered. This brought us to explore gradient-based search approaches, thanks to a differentiable relaxation of the initial problem.

In this paper, we extend the bilevel framework of AutoAugment [9] in order to search for class-wise data augmentation policies. We demonstrate on digit classification and sleep staging tasks that class-wise augmentation allows to find some interesting invariances and to improve prediction performance. In order to cope with the much larger search space induced by the class-wise policies, we propose CADDA, a novel automatic augmentation method which aims to directly solve the bilevel problem using a gradient-based method. This method is evaluated on EEG, for which we propose three novel augmentation transformations shown to outperform most previously proposed ones. Our method leads to significant speed up compared to four other state-of-the-art automatic augmentation strategies, while reaching top performance. Our experiments confirm [12] that density matching-based approaches [13, 14] are not competitive.

2 Related Work

EEG Data Augmentation The interest in using deep learning for EEG related tasks has been rapidly growing in the last years, specially for applications in sleep staging, seizure detection and prediction, and brain-computer interfaces (BCI) [15]. Given the relatively small size of available EEG datasets, part of the community has explored ways of generating more data from existing ones, *e.g.*, using generative models [16, 17] or data augmentation strategies [18, 19, 20, 21, 22, 23, 24, 25].

The most basic form of data augmentation proposed is the addition of white noise to EEG signals [21] or to derived features [18]. This transformation has the advantage of modifying the waveform shapes in the time domain, while moderately distorting the proportions of different frequencies in the signals spectra. It indeed adds the same power to all frequencies equally. It should hence work as an augmentation for tasks where the predictive information is well captured by frequency-bands power ratios, as used for pathology detection in [26].

Another type of augmentation are time related transformations, such as time shifting and time masking [24] (a.k.a. time cutout [23]). Both aim to make the predictions more robust, the latter supposing that

the label of an example must depend on the overall signal, and the former trying to teach the model that misalignment between human-annotations and events should be tolerated up to some extent.

Similarly, transformations acting purely in the frequency domain have been proposed. Just as time masking zeros-out a small portion of the signal in the time domain, narrow bandstop filtering at random spectra positions [23, 24] attempts to prevent the model from relying on a single frequency band. Another interesting frequency data augmentation is the FT-surrogate transform [22]. It consists in replacing the phases of Fourier coefficients by random numbers sampled uniformly from $[0, 2\pi)$. The authors of this transformation assume that portions of EEG signals can be approximated by linear stationary processes, which are known to be uniquely defined by their Fourier amplitudes.

Another widely explored type of EEG data augmentation are spatial transformations, acting on sensors positions. For example, sensors are rotated and shifted in [19], to simulate small perturbations on how the sensors cap is placed on the head. Likewise, the brain bilateral symmetry is exploited in [20], where the left and right-side signals are switched. Sensors cutout (*i.e.*, zeroing-out signals of sensors in a given zone) is studied in [23], while [25] propose to randomly drop or shuffle channels to increase the model robustness to differences in the experimental setting. Mixing signals from different examples has also been suggested in [24].

The reader is referred to [15] for a more in-depth systematic review of existing EEG data augmentation papers. In this work we have explored most of the augmentations described above. To our knowledge, this work is the first to carry an ambitious comparison of data augmentation techniques for sleep staging, and to investigate automatic approaches in EEG deep learning pipelines.

Automatic Data Augmentation Let D_{train} and D_{valid} denote a training and validation set respectively, and let \mathcal{T} be an augmentation policy, as defined in more detail in Section 4. Automatic data augmentation is about finding algorithms solving the following bilevel optimization problem:

$$\begin{aligned} \min_{\mathcal{T}} \quad & \mathcal{L}(\theta^* | D_{\text{valid}}) \\ \text{s.t.} \quad & \theta^* \in \arg \min_{\theta} \mathcal{L}(\theta | \mathcal{T}(D_{\text{train}})), \end{aligned} \tag{1}$$

where θ denotes the parameters of some predictive model, and $\mathcal{L}(\theta | D)$ its loss over set D . In other words, it is about searching augmentations that, when applied during the model training, will minimize its loss over the validation set, leading to greater generalization on some hidden test set.

One of the first influential works in this area is AutoAugment [9], where problem (1) is solved by fully training multiple times a smaller model on a subset of the training set with different augmentation policies and using the validation loss as a reward function in a reinforcement learning setting. The main drawback of the method is its enormous computation cost. Many alternative methods have been proposed since, differing mainly in terms of search space, algorithm in charge of looking for new candidate policies and metric used to assess each candidate policy.

The first attempts to make AutoAugment more efficient consisted in carrying the model and policy trainings jointly, leading to learnt augmentation policy schedules rather than fixed policies. In Population-Based Augmentation [7], a genetic algorithm is used to train a population of models with different policies, making the best models and augmentation policies share their parameters with the worst ones every fixed number of epochs. Joint training is also explored in [27], where policies are modeled as parametrized distributions over possible transformations and learnt online. As augmentations are sampled during training, the distribution parameters are updated using the REINFORCE algorithm [28]. Similarly, Adversarial AutoAugment [29] uses this same trick to backpropagate through an augmentation policy model. It is however done in an adversarial way, with an augmentation network that tries to make the model training hard, by maximizing the training loss.

A different way of alleviating the computation burden of AutoAugment is proposed in [12]. Observing that most of the gains obtained by custom data augmentation happen at the end of training, the authors propose to pre-train a shared model close to convergence with augmentations sampled uniformly, and then to use it to warmstart the AutoAugment iterations for fine-tuning.

The previous methods [9, 7, 13] use proxy tasks with small models and training subsets to carry the search. This idea is challenged in RandAugment [8], where it is shown that optimal augmentations highly depend on the dataset size and the model. RandAugment reduces the search space drastically and simply samples augmentations uniformly with the same shared magnitude, which can be tuned with a grid-search. Competitive results are obtained on computer vision tasks with this naive policy.

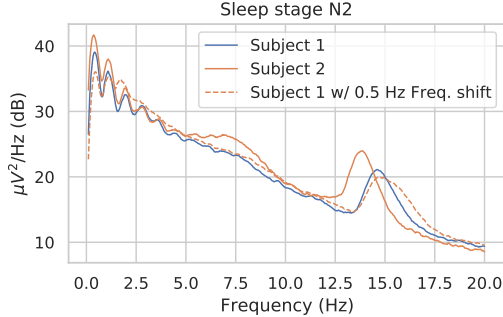


Figure 1: Averaged power spectral density of N2 windows from one night sleep of two different subjects from the sleep Physionet dataset (channel Pz-Oz used here) [35]. We notice that peak frequencies are shifted. Applying a 0.5 Hz frequency shift transform to subject 1 leads a power spectrum density more similar to subject 2.

While all previously cited methods try to solve in some sense the original problem (1), Fast AutoAugment [13] suggests to solve a surrogate problem, by moving the policy \mathcal{T} into the upper-level:

$$\begin{aligned} \min_{\mathcal{T}} \quad & \mathcal{L}(\theta^* | \mathcal{T}(D_{\text{valid}})) \\ \text{s.t.} \quad & \theta^* \in \arg \min_{\theta} \mathcal{L}(\theta | D_{\text{train}}) . \end{aligned} \tag{2}$$

Problem (2) can be seen as a form of ‘density matching’ [13], where we look for augmentation policies such that the augmented validation set has the same distribution as the training set, as evaluated through the lens of the trained model. This greatly simplifies problem (1) which is no longer bilevel, allowing to train the model only once without augmentation. Computation is massively reduced, yet this simplification assumes the trained model has already captured meaningful invariances.

This density matching objective has been later reused in Faster AutoAugment [14], where backpropagation is used to solve problem (2) instead of the gradient-free Tree-Parzen Estimator [30]. Also, instead of using the trained classifier to assess the closeness between augmented and original data distributions, this work uses a Wasserstein GAN network [31] as a critic. Unlike [12, 29], where REINFORCE is used to estimate gradients, [14] derives a full continuous relaxation of the original formalism of AutoAugment, which we build on in this work. The authors got their inspiration from DARTS [32], where a similar relaxation is used to carry Neural Architecture Search (NAS) using gradients. This work revisits [32] in Section 4.3, adapting the gradient approximation proposed.

Class-dependent Data Augmentation While class-dependent data generation has been studied in the GAN literature [33], to our knowledge, [34] is the only work that has explored class-dependent data augmentations. It presents a method for learning a distribution of class-wise spatial distortions, by training a model to find the C^1 -diffeomorphism allowing to transform one example into another within the same class. Although the authors state it is applicable to other domains, it is only demonstrated for digit classification and its extension to other frameworks seems non-trivial. The main difference with our work is that [34] learns transformations from scratch, while we try to learn which one to pick from a pool of existing operations and how to aggregate them.

3 New EEG data augmentations

In addition to the data augmentations described in Section 2, we investigate in this paper three novel operations acting on the time, space and frequency domains. These transforms are described below.

Time Reverse As a new time domain transformation, we propose to randomly reverse time in certain input examples (*i.e.*, flip the time axis of the signal). Our motivation is the belief that most of the sleep stage information encoded in EEG signals resides in relative proportions of frequencies and in the presence of certain prototypical short waves. On this last point, it is possible that not all sleep stages are invariant to this transform, as some important waves (*e.g.*, K-complexes) are asymmetric and are therefore potentially altered by the transformation.

Sign Flip In the spatial transformations category, we argue that the information encoded in the electrical potentials captured by EEG sensors are likely to be invariant to the polarity of the electric field. Given the physics of EEG, the polarity of the field is defined by the direction of the flow of electric charges along the neuron dendrites: are charges moving towards deeper layers of the cortex

or towards superficial ones? As both are likely to happen in a brain region, we propose to augment EEG data by randomly flipping the signals sign (multiplying all channels’ outputs by -1).

Frequency Shift Reading the sleep scoring manual [11], it is clear that dominant frequencies in EEG signals play an important role in characterising different sleep stages. For instance, it is said that the N2 stage can be recognized by the presence of sleep spindles between 11-16 Hz. Such frequency range is quite broad, and when looking at the averaged power spectral density of windows in this stage for different individuals, one can notice that the frequency peaks can be slightly shifted (*cf.* Figure 1). To mimic this phenomena we propose to shift the frequencies of signals fragments by an offset Δf sampled uniformly from a small range (See Appendix A.1 for details).

4 Class-wise Automatic Differentiable Data Augmentation

We adopt the same framework of definitions from AutoAugment [9], which was also reused in [7, 12, 13, 14]. Let \mathcal{X} denote the inputs space. We define an *augmentation operation* \mathcal{O} as a mapping from \mathcal{X} to \mathcal{X} , depending on a magnitude parameter μ and a probability parameter p . While μ specifies how strongly the inputs should be transformed, p sets the probability of actually transforming them:

$$\mathcal{O}(X; p, \mu) := \begin{cases} \mathcal{O}(X; \mu) & \text{with probability } p \text{ ,} \\ X & \text{with probability } 1 - p \text{ .} \end{cases} \quad (3)$$

Operations can be applied sequentially, forming what we call an *augmentation subpolicy* of length K :

$$\tau(X; \mu_\tau, p_\tau) := (\mathcal{O}_K \circ \dots \circ \mathcal{O}_1)(X; \mu_\tau, p_\tau),$$

where μ_τ and p_τ denote the concatenation of the K operations parameters. To increase the randomness of the augmentation strategy, L subpolicies are grouped into a set called an *augmentation policy* \mathcal{T} , from which they are sampled with uniform probability for each new batch of inputs:

$$\mathcal{T}(X) = \tau_i(X; \mu_{\tau_i}, p_{\tau_i}), \quad \text{with } i \sim \mathcal{U}(\{1, \dots, L\}).$$

Note that some operations, such as the *Time Reverse* and *Sign Flip* augmentations described in Section 3, may not depend on a magnitude parameter, which reduces the search space.

Class-wise subpolicies We introduce in this paper augmentation subpolicies which are conditioned on the input class. Hence, we define a *class-wise subpolicy* as a mapping between inputs X and labels y to an augmentation subpolicy τ_y :

$$\tilde{\tau} : (X, y) \mapsto \tau_y(X)$$

where $\{\tau_y : y \in \mathcal{Y}\}$ is a set of subpolicies for each possible class in the output space \mathcal{Y} .

4.1 Illustration of the usefulness of class-wise augmentation on MNIST

Motivation In order to illustrate the potential of class-wise augmentation, we present in this section a simple example using the MNIST dataset [36]. Intuitively, some common image augmentation operations such as horizontal flips or rotations with large angles should not be helpful for handwritten digits recognition: if you rotate a 9 too much, it might be difficult to distinguish it from a 6. However, some digits have more invariances than others. For example, 0’s and 8’s are relatively invariant to vertical and horizontal flips, as well as to 180 degrees rotations. We used this framework to compare a naive approach of automatic data augmentation search both in a standard and in a class-wise setting.

Algorithm For simplicity, we used a random search algorithm to look for augmentation policies, with operations’ parameters discretized over a grid. More precisely, each new candidate subpolicy sampled by the search algorithm is used to train the model from scratch, before evaluating it on the validation set. In terms of search space and search metric, this is equivalent to what is done in AutoAugment [9], although the reinforcement learning algorithm is replaced by random sampling.

Search space Let N_p , N_μ and $N_{\mathcal{O}}$ denote the number of possible probability, magnitude values and operations in our setting. The search space of both standard and class-wise policies is potentially huge: $(N_p \times N_\mu \times N_{\mathcal{O}})^{L \times K \times |\mathcal{Y}|}$, where the number of classes $|\mathcal{Y}|$ is replaced by 1 in the standard case. Given the simplicity of the algorithm used, we tried to reduce the search space as much as

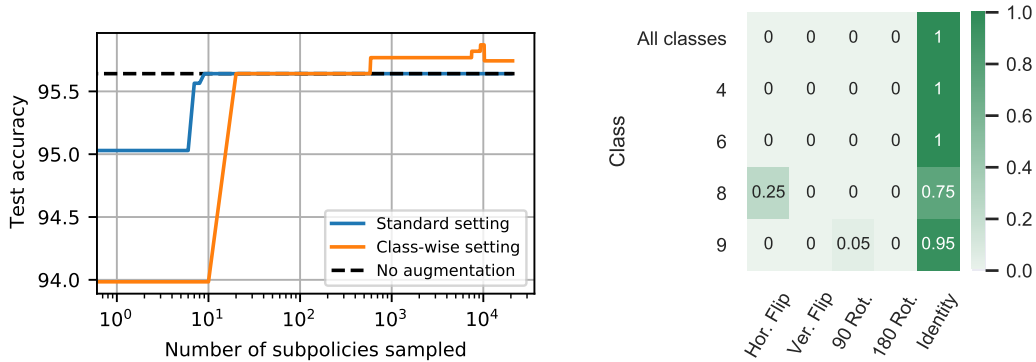


Figure 2: **(left)** Test accuracy obtained using the subpolicy with higher performance on validation set. **(right)** Probability of applying each operation in the best policy found ($L = 5$). First row corresponds to the standard setting and following rows to the class-wise setting.

possible. Hence, we only considered subpolicies of length $K = 1$ (a single operation) and restrained our problem to the classification of 4 digits only: 4, 6, 8 and 9. A pool of four transformations that only depend on a probability parameter (no magnitude) was used in the search: horizontal and vertical flip, as well as 90 and 180 degrees rotation (counter-clockwise).

Despite this significant simplification, the search space size for policies made of $L = 5$ subpolicies is still immense: around 10^6 for standard policies and 1.2×10^{24} for class-wise policies. For this reason, 20,000 trials were sampled in both cases. As an additional baseline, we also trained the same model without any type of data augmentation.

Experimental setting After the 4-class reduction, the MNIST training set was randomly split into a training set containing 1000 images per class and a validation set of 3000 images per class. The reduced MNIST test set used to evaluate the final performance has 1000 images per class, as the original one. All transforms were implemented using torchvision [37]. We used the LeNet-1 architecture [36] for the classifier. It was trained using batches of 64 images and Adam optimizer [38] with an initial learning rate of 2×10^{-3} , $\beta_1 = 0.9$, $\beta_2 = 0.999$ and no weight decay. Trainings had a maximum number of 50 epochs and were early-stopped with a patience of 5 epochs.

Results As seen on Figure 2, random search converges to the identity policy (no augmentation). This was expected as none of the available operations describe an invariance shared by all four digits. From Figure 2-right we see that the class-wise random search does not find a good augmentation for digits 4 and 6 as well. Yet, it is able to recover that digit 8 is invariant to horizontal flip. Interestingly, 90 degree rotation of digit 9 is also selected with a small probability. This can be understood, as some people might draw the 9’s leg more horizontally than others, so that rotating up to 90 degrees counter-clockwise still preserves in some cases the picture semantics. Figure 2-left shows that the class-wise algorithm can find interesting policies in such a constrained setting, but also that it can outperform the baselines. Yet, this happens only after 10,000 trials.

This toy experiment suggests that looking for augmentation strategies depending on the label of the data being transformed can be relevant to improve prediction performance, but also to help discovering some interesting invariances for the task considered. However, despite the extremely simplified setting used, the class-wise search took 14.4 GPU days (Tesla V100 SXM2). It becomes clear that a more efficient search strategy is required for real-world applications.

4.2 Differentiable Augmentation Policies

As explained in Faster AutoAugment [14], while automatic data augmentation is about optimizing a policy model on a huge search space, most existing approaches are based on gradient-free algorithms, mainly because the problem is cast in a discrete setting. For this reason, they propose a continuous relaxation of the automatic augmentation problem, inspired by a recent NAS method: DARTS [32]. Hereafter we build on these relaxation ideas in the EEG setting.

Probabilities Equation (3) can be rewritten as follows:

$$\mathcal{O}(X; p, \mu) = b\mathcal{O}(X; \mu) + (1 - b)X, \quad (4)$$

where b is sampled from a Bernoulli distribution with probability p . Doing so, Equation (4) can be made differentiable with respect to p by using a Relaxed Bernoulli [39], *i.e.*, by reparametrizing the distribution as a continuous function depending on p and on a uniform random variable [40].

Magnitudes While some operations don't depend on any magnitude parameter, most of the augmentations described in section Section 2 do and are not differentiable with respect to it. In [14] it is argued that using a simple *straight-through gradient estimator* [39] is enough to face this difficulty (*i.e.*, approximating the gradient of $\mathcal{O}(X; \mu)$ w.r.t μ by 1).

In practice, we found that this approach alone did not allow to properly transmit the gradient loss information to tune the magnitudes. For this reason, we preferred to carry out a case-by-case relaxation of each operations considered. The detailed implementation of these relaxations can be found in Section A.1, but all of them shared the same principles listed below:

1. when μ is used to set some sampling operation, a pathwise gradient estimator is used [40], just as for p in Eq. (4);
2. when some masking is necessary, vector indexing is replaced by element-wise multiplications between the transformed vector and a smooth mask built using sigmoid functions;
3. the straight-through estimator is only used to propagate the gradient through the permutation operation in `channel_shuffle`.

Operations During search, operations need to be selected over a discrete set. As in Faster AutoAugment [14], we replace the sequence of sampled operations in a subpolicy by a sequence of stages $\{\tilde{\mathcal{O}}_k : k = 1, \dots, K\}$, which are a convex combination of all operations:

$$\tilde{\mathcal{O}}_k(X) = \sum_{n=1}^{N_{\mathcal{O}}} [\sigma_{\eta}(w_k)]_n \mathcal{O}_k^{(n)}(X; \mu_k^{(n)}, p_k^{(n)}),$$

where w_k denote the weights vector of stage k . These weights are passed through a softmax activation σ_{η} , so that, when parameter η is small, $\sigma_{\eta}(w_k)$ becomes a onehot-like vector.

At inference time, while in Faster AutoAugment the operation applied at each stage is sampled from the weights distribution, we choose to always pick the operation corresponding to the maximum weight. This way, our subpolicies have the same structure as in AutoAugment at the end of the search.

4.3 Policy Gradient Estimation

The inspiration of Faster AutoAugment [14] regarding DARTS [32] comes probably from the fact that both automatic augmentation and NAS share many similarities: both are optimization problems originally cast in discrete settings and both have a bilevel structure (Eq. (1)). However, while in DARTS the bilevel problem of interest is solved directly, Faster AutoAugment casts a surrogate density matching problem. While this surrogate problem is easier and faster to solve, [12] presents empirical evidence suggesting that the density matching metric is not really correlated to what is really meant to be optimized in problem (1). Indeed, we confirmed these results to some extent in our experiments (*cf.* Section 5). Here, we propose to build on DARTS to actually tackle the bilevel optimization from (1). Let α be the vector grouping all the parameters of a continuously relaxed policy model \mathcal{T}_{α} as described in Section 4.2. We carry alternating optimization steps of the policy

Algorithm 1: CADDA

Input : $\xi, \epsilon > 0$, Datasets $D_{\text{train}}, D_{\text{valid}}$,
Trainable policy \mathcal{T}_{α} , Model θ

Result: Policy parameters α

while not converged do

// compute the unrolled model

$g_{\theta} = \mathcal{L}(\theta | \mathcal{T}_{\alpha}(D_{\text{train}})).\text{backward}(\theta)$

$\theta' := \theta - \xi g_{\theta}$

// Estimate $\nabla_{\alpha} \mathcal{L}(\theta' | D_{\text{valid}})$

$g'_{\theta} = \mathcal{L}(\theta' | D_{\text{valid}}).\text{backward}(\theta)$

$g_{\alpha}^{+} = \mathcal{L}(\theta + \epsilon g'_{\theta} | \mathcal{T}_{\alpha}(D_{\text{train}})).\text{backward}(\alpha)$

$g_{\alpha}^{-} = \mathcal{L}(\theta - \epsilon g'_{\theta} | \mathcal{T}_{\alpha}(D_{\text{train}})).\text{backward}(\alpha)$

$g_{\alpha} = \frac{1}{2\epsilon}(g_{\alpha}^{+} - g_{\alpha}^{-})$

// Update Policy parameters α

$\alpha = \alpha - \xi g_{\alpha}$

// Update the model parameters θ

$g_{\theta} = \mathcal{L}(\theta | \mathcal{T}_{\alpha}(D_{\text{train}})).\text{backward}(\theta)$

$\theta = \theta - \xi g_{\theta}$

end

parameters α and the model parameters θ . In order to estimate the augmentation policy gradient, we approximate the lower-level of (1) by a single optimization step:

$$\nabla_{\alpha} \mathcal{L}(\theta^* | D_{\text{valid}}) \simeq \nabla_{\alpha} \mathcal{L}(\theta' | D_{\text{valid}}), \quad \text{with } \theta' := \theta - \xi \nabla_{\theta} \mathcal{L}(\theta | \mathcal{T}_{\alpha}(D_{\text{train}})), \quad (5)$$

where ξ denotes the learning rate. By applying the chain rule in Equation (5) we get:

$$\nabla_{\alpha} \mathcal{L}(\theta' | D_{\text{valid}}) = -\xi \nabla_{\alpha, \theta}^2 \mathcal{L}(\theta | \mathcal{T}_{\alpha}(D_{\text{train}})) \nabla_{\theta'} \mathcal{L}(\theta' | D_{\text{valid}}) \quad (6)$$

$$\simeq -\xi \frac{\nabla_{\alpha} \mathcal{L}(\theta^+ | \mathcal{T}_{\alpha}(D_{\text{train}})) - \nabla_{\alpha} \mathcal{L}(\theta^- | \mathcal{T}_{\alpha}(D_{\text{train}}))}{2\epsilon}, \quad (7)$$

where ϵ is a small scalar and $\theta^{\pm} = \theta \pm \epsilon \nabla_{\theta} \mathcal{L}(\theta' | D_{\text{valid}})$. The second line (7) corresponds to a finite difference approximation of the Hessian-gradient product. Note that unlike in NAS, the first element in (6) is 0 in our case because the upper-level of problem (1) does not depend directly on α .

5 Experiments on EEG data during sleep

Datasets We used the public dataset MASS - Session 3 [41]. It corresponds to 62 nights, each one coming from a different subject. Out of the 20 available EEG channels, referenced with respect to the A2 electrode, we used 6 (C3, C4, F3, F4, O1, O2). We also used the standard sleep Physionet data [35] which contains 153 recordings from 83 subjects. Here two EEG derivations are available (FPz-Cz and Pz-Oz). For both datasets, sleep stages were annotated according to the AASM rules [10]. The EEG time series were first lowpass filtered at 30 Hz (with 7 Hz transition bandwidth). Then for MASS they were resampled from 256 Hz to 128 Hz. The Physionet dataset was kept at 100 Hz.

Experimental details The architecture used for learning is the convolutional network proposed in [42]. The optimizer used was Adam with a learning rate of 10^{-3} , $\beta_1 = 0$. and $\beta_2 = 0.999$. At most 300 epochs were used for training. Early stopping was implemented with a patience of 30 epochs. Balanced accuracy was used as performance metric using the inverse of original class frequencies as balancing weights. The MNE-Python [43] and Braindecode software [44] were used to preprocess and learn on the EEG data. Training was carried on single Tesla V100 GPUs.

Manual exploration All EEG data augmentation techniques were first tested individually without automatic search strategy on the two datasets, using a batch size of 128. Datasets were split in 5 folds with 16 subjects for Physionet and 12 subjects for MASS in a test set. Among the training folds, data were split in 80/20 randomly to obtain a training and a validation set. To assess the effect of augmentation at different data regimes, the training set was sequentially subset using a log2 scale (with stratified splits). All augmentations tested had 0.5 probability and a manually fine-tuned magnitude (*cf.* Section A.2). Results on the two datasets are presented in Figure 3 and Figure 4. As expected, augmentation plays a major role in the low data regime. Transforms like FT and Frequency Shift lead to up to 60% performance improvement on the test set for MASS in extremely low data regimes. Surprisingly, rotations and time masking do not seem to help a lot.

Automatic search As commonly done [9, 7, 13, 14], we considered policies of size $L = 5$, made of subpolicies of length $K = 2$. The (C)ADDA approaches are compared to 4 alternative strategies: standard and class-wise random search (100 trials), Fast AA (200 trials ; implemented with optuna [45]), and Faster AA (reproduced from original authors code) using 20 epochs. The MASS dataset was used for this experiment. Training was carried on 1 night of sleep using a batch size of 16. The validation set consisted of 47 nights.

For each method, we stopped the search every given number of steps (detailed in Section A.4), used the learnt policy to retrain from scratch the model on the training set (leading to a point in Figure 5) and resumed the search from where it stopped. For each run, when the final retraining validation accuracy improves compared to previous retraining, we report the new test accuracy obtained by the retrained model (otherwise, we keep the previous value). We see that while passing to the class-wise setting significantly hurts the gradient-free methods (random search), CADDA conserves its efficiency. Figure 6 shows the selected transforms by the different techniques. We see that, unlike density matching approaches, top performing methods have selected the same winning transformations found by the manual search. See Appendix A.4 for complementary figures.

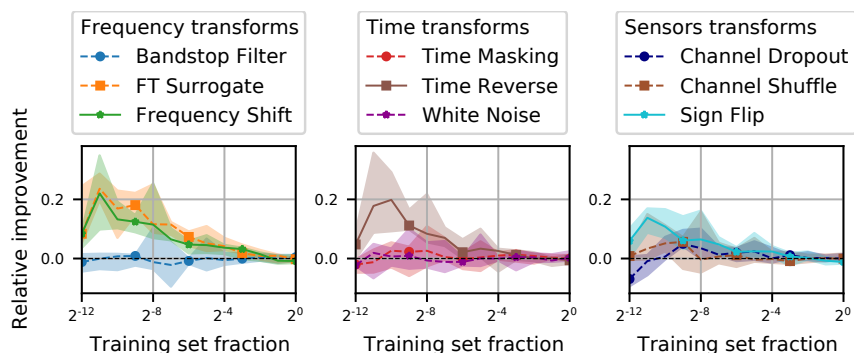


Figure 3: Median performance gains obtained by individual augmentation strategies on the Physionet dataset while increasing the train set size. Results are relative improvements compared to the baseline without any augmentation. Two frequency transforms (FT Surrogate and Frequency shift) as well as the Time Reverse transform lead to best relative improvements compared to the baseline obtained without any augmentation. Using more training data mitigates the need for data augmentation.

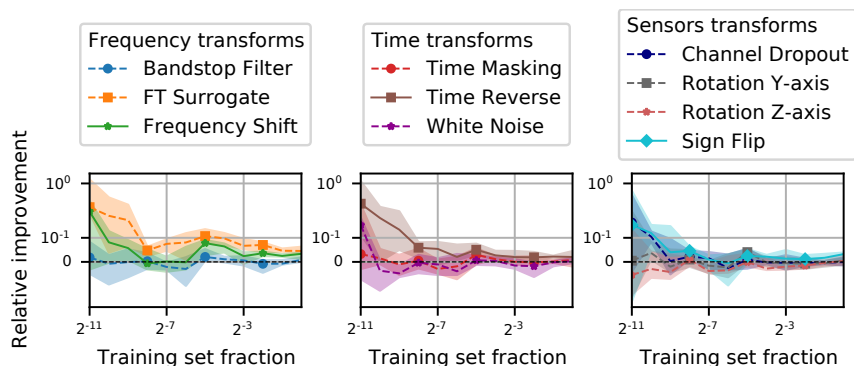


Figure 4: Median performance gains obtained by individual augmentation strategies on the MASS dataset. Best transforms obtained on Physionet (*cf.* Fig. 3) give here consistent improvements, while sensors transformation like Channel Dropout are more relevant when using 6 channels. Here also using more training data mitigates the need for data augmentation.

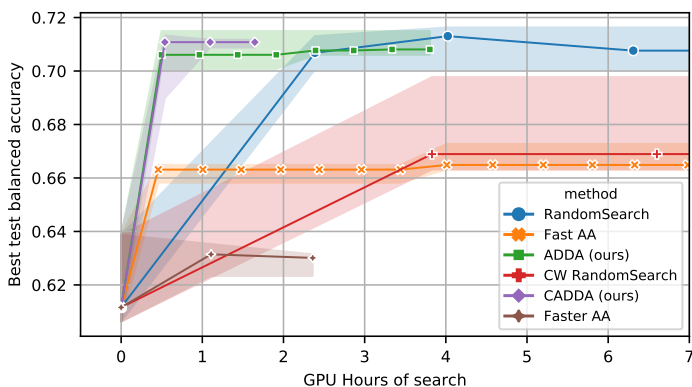


Figure 5: Median performance obtained by different automatic data augmentation strategies as a function of the computation time. CADDA and ADDA reach top performance faster than random search with a small margin for CADDA. Approaches based on density matching fail to learn relevant augmentation policies and are not competitive.



Figure 6: Probability of applying each operation in the best policies obtained by the different search strategies. For each method, probabilities of all subpolicies are grouped. Methods based on differentiable augmentation policies discover relevant augmentation strategies such as Time Reverse, Sign Flip, FT surrogate etc. CADDA suggests that each class benefits differently from the different strategies.

Acknowledgments and Disclosure of Funding

This work was supported by the BrAIN grant (ANR-19-DATA-0023). It was also granted access to the HPC resources of IDRIS under the allocation 2021-AD011012284 and 2021-AD011011172R1 made by GENCI.

References

- [1] Alex Krizhevsky, Ilya Sutskever, and Geoffrey E. Hinton. ImageNet classification with deep convolutional neural networks. In *Advances in neural information processing systems*, volume 25, pages 1097–1105, 2012.
- [2] Larry S Yaeger, Richard F Lyon, and Brandyn J Webb. Effective Training of a Neural Network Character Classifier for Word Recognition. In *Advances in neural information processing systems*, volume 9, pages 807–816, 1996.
- [3] Patrice Y. Simard, Dave Steinkraus, and John C. Platt. Best practices for convolutional neural networks applied to visual document analysis. In *International Conference on Document Analysis and Recognition*, volume 3, pages 958–963, 2003.
- [4] Shuxiao Chen, Edgar Dobriban, and Jane H Lee. A Group-Theoretic Framework for Data Augmentation. In *Neural Information Processing Systems*, 2020.
- [5] Laurens van der Maaten, Minmin Chen, Stephen Tyree, and Kilian Q. Weinberger. Learning with Marginalized Corrupted Features. In *Proceedings of the 30th International Conference on Machine Learning*, volume 28, page 9, 2013.
- [6] Ting Chen, Simon Kornblith, Mohammad Norouzi, and Geoffrey Everest Hinton. A simple framework for contrastive learning of visual representations. *CoRR*, 2020.
- [7] Daniel Ho, Eric Liang, Ion Stoica, Pieter Abbeel, and Xi Chen. Population Based Augmentation: Efficient Learning of Augmentation Policy Schedules. In *International Conference on Machine Learning (ICML)*, pages 2731–2741, Vienna, Austria, May 2019. PMLR. arXiv: 1905.05393.
- [8] Ekin D. Cubuk, Barret Zoph, Jonathon Shlens, and Quoc V. Le. Randaugment: Practical automated data augmentation with a reduced search space. In *IEEE/CVF Conference on Computer Vision and Pattern Recognition Workshops (CVPRW)*, pages 3008–3017, Seattle, WA, USA, June 2020. IEEE.
- [9] Ekin D. Cubuk, Barret Zoph, Dandelion Mane, Vijay Vasudevan, and Quoc V. Le. AutoAugment: Learning Augmentation Strategies From Data. In *IEEE/CVF Conference on Computer Vision and Pattern Recognition (CVPR)*, pages 113–123, Long Beach, CA, USA, June 2019. IEEE.
- [10] C. Iber, S. Ancoli-Israel, A. Chesson, and S. F. Quan. The AASM Manual for the Scoring of Sleep and Associated Events: Rules, Terminology and Technical Specification, 2007.
- [11] Richard S. Rosenberg and Steven Van Hout. The American Academy of Sleep Medicine Inter-scoring Reliability Program: Sleep Stage Scoring. *Journal of Clinical Sleep Medicine : JCSM : Official Publication of the American Academy of Sleep Medicine*, 9(1):81–87, January 2013.
- [12] Keyu Tian, Chen Lin, Ming Sun, Luping Zhou, Junjie Yan, and Wanli Ouyang. Improving Auto-Augment via Augmentation-Wise Weight Sharing. In *Advances in Neural Information Processing Systems*, volume 33, pages 19088–19098, 2020.
- [13] Sungbin Lim, Ildoo Kim, Taesup Kim, Chiheon Kim, and Sungwoong Kim. Fast AutoAugment. In *Advances in Neural Information Processing Systems (NeurIPS)*, pages 6665–6675, Vancouver, BC, Canada, 2019.
- [14] Ryuichiro Hataya, Jan Zdenek, Kazuki Yoshizoe, and Hideki Nakayama. Faster AutoAugment: Learning Augmentation Strategies Using Backpropagation. In Andrea Vedaldi, Horst Bischof, Thomas Brox, and Jan-Michael Frahm, editors, *Computer Vision – ECCV 2020*, pages 1–16, Cham, 2020. Springer International Publishing.
- [15] Yannick Roy, Hubert Banville, Isabela Albuquerque, Alexandre Gramfort, Tiago H Falk, and Jocelyn Faubert. Deep learning-based electroencephalography analysis: a systematic review. *Journal of Neural Engineering*, 16(5):051001, August 2019.
- [16] Kay Gregor Hartmann, Robin Tibor Schirrmeyer, and Tonio Ball. EEG-GAN: Generative adversarial networks for electroencephalographic (EEG) brain signals. *arXiv:1806.01875*, June 2018. arXiv: 1806.01875.
- [17] G. Bouallegue and R. Djemal. EEG data augmentation using Wasserstein GAN. In *2020 20th International Conference on Sciences and Techniques of Automatic Control and Computer Engineering (STA)*, pages 40–45, December 2020. ISSN: 2573-539X.

- [18] Zhong Yin and Jianhua Zhang. Cross-session classification of mental workload levels using EEG and an adaptive deep learning model. *Biomedical Signal Processing and Control*, 33:30–47, March 2017.
- [19] Mario Michael Krell and Su Kyoung Kim. Rotational data augmentation for electroencephalographic data. In *2017 39th Annual International Conference of the IEEE Engineering in Medicine and Biology Society (EMBC)*, pages 471–474, Seogwipo, July 2017. IEEE.
- [20] Olivier Deiss, Siddharth Biswal, Jing Jin, Haoqi Sun, M. Brandon Westover, and Jimeng Sun. HAMLET: Interpretable Human And Machine co-LEarning Technique. *arXiv:1803.09702*, August 2018. *arXiv: 1803.09702*.
- [21] Fang Wang, Sheng-hua Zhong, Jianfeng Peng, Jianmin Jiang, and Yan Liu. Data Augmentation for EEG-Based Emotion Recognition with Deep Convolutional Neural Networks. In *MultiMedia Modeling*, volume 10705, pages 82–93. Springer International Publishing, 2018. Series Title: Lecture Notes in Computer Science.
- [22] Justus T. C. Schwabedal, John C. Snyder, Ayse Cakmak, Shamim Nemati, and Gari D. Clifford. Addressing Class Imbalance in Classification Problems of Noisy Signals by using Fourier Transform Surrogates. *arXiv:1806.08675*, 2019. *arXiv: 1806.08675*.
- [23] Joseph Y. Cheng, Hanlin Goh, Kaan Dogrusoz, Oncel Tuzel, and Erdin Azemi. Subject-Aware Contrastive Learning for Biosignals. *arXiv:2007.04871*, June 2020. *arXiv: 2007.04871*.
- [24] Mostafa Mohsenvand, Mohammad Rasool Izadi, and Pattie Maes. Contrastive Representation Learning for Electroencephalogram Classification. In *Machine Learning for Health*, 2020.
- [25] Aaqib Saeed, David Grangier, Olivier Pietquin, and Neil Zeghidour. Learning From Heterogeneous Eeg Signals with Differentiable Channel Reordering. In *ICASSP 2021 - 2021 IEEE International Conference on Acoustics, Speech and Signal Processing (ICASSP)*, pages 1255–1259, June 2021. ISSN: 2379-190X.
- [26] Lukas A.W. Gemein, Robin T. Schirrmeyer, Patryk Chrabaszcz, Daniel Wilson, Joschka Boedecker, Andreas Schulze-Bonhage, Frank Hutter, and Tonio Ball. Machine-learning-based diagnostics of eeg pathology. *NeuroImage*, 220:117021, 2020.
- [27] Chen Lin, Minghao Guo, Chuming Li, Xin Yuan, Wei Wu, Junjie Yan, Dahua Lin, and Wanli Ouyang. Online Hyper-Parameter Learning for Auto-Augmentation Strategy. In *2019 IEEE/CVF International Conference on Computer Vision (ICCV)*, pages 6578–6587, Seoul, Korea (South), October 2019. IEEE.
- [28] Ronald J Williams. Simple statistical gradient-following algorithms for connectionist reinforcement learning. *Machine learning*, 8(3-4):229–256, 1992.
- [29] Xinyu Zhang, Qiang Wang, Jian Zhang, and Zhao Zhong. Adversarial AutoAugment. *arXiv:1912.11188 [cs, stat]*, December 2019. *arXiv: 1912.11188*.
- [30] James S Bergstra, Rémi Bardenet, Yoshua Bengio, and Balázs Kégl. Algorithms for Hyper-Parameter Optimization. In *Advances in Neural Information Processing Systems*, volume 24, page 9, 2011.
- [31] Martin Arjovsky, Soumith Chintala, and Leon Bottou. Wasserstein Generative Adversarial Networks. In *Proceedings of the 34th International Conference on Machine Learning*, volume 70 of *Proceedings of Machine Learning Research*, pages 214–223, 2017.
- [32] Hanxiao Liu, Karen Simonyan, and Yiming Yang. DARTS: Differentiable Architecture Search. In *International Conference on Learning Representations*, 2019.
- [33] Mehdi Mirza and Simon Osindero. Conditional Generative Adversarial Nets. *arXiv:1411.1784*, November 2014. *arXiv: 1411.1784*.
- [34] Søren Hauberg, Oren Freifeld, and Anders Boesen Lindbo Larsen. Dreaming More Data: Class-dependent Distributions over Diffeomorphisms for Learned Data Augmentation. In *Artificial Intelligence and Statistics*, pages 342–350, 2016.
- [35] Ary L Goldberger, Luis AN Amaral, Leon Glass, Jeffrey M Hausdorff, Plamen Ch Ivanov, Roger G Mark, Joseph E Mietus, George B Moody, Chung-Kang Peng, and H Eugene Stanley. PhysioBank, PhysioToolkit, and PhysioNet: components of a new research resource for complex physiologic signals. *Circulation*, 101(23):e215–e220, 2000.
- [36] Yann LeCun, Léon Bottou, Yoshua Bengio, and Patrick Haffner. Gradient-based learning applied to document recognition. *Proceedings of the IEEE*, 86(11):2278–2324, 1998.
- [37] Sébastien Marcel and Yann Rodriguez. Torchvision the Machine-Vision Package of Torch. In *Proceedings of the 18th ACM International Conference on Multimedia*, pages 1485–1488. Association for Computing Machinery, 2010.
- [38] Diederik P. Kingma and Jimmy Ba. Adam: A Method for Stochastic Optimization. In Yoshua Bengio and Yann LeCun, editors, *3rd International Conference on Learning Representations, ICLR 2015, San Diego, CA, USA, May 7-9, 2015, Conference Track Proceedings*, 2015.

- [39] Yoshua Bengio, Nicholas Léonard, and Aaron C. Courville. Estimating or Propagating Gradients Through Stochastic Neurons for Conditional Computation. *CoRR*, 2013.
- [40] John Schulman, Nicolas Heess, Theophane Weber, and Pieter Abbeel. Gradient Estimation Using Stochastic Computation Graphs. In C. Cortes, N. Lawrence, D. Lee, M. Sugiyama, and R. Garnett, editors, *Advances in Neural Information Processing Systems*, volume 28, 2015.
- [41] Christian O’reilly, Nadia Gosselin, Julie Carrier, and Tore Nielsen. Montreal archive of sleep studies: an open-access resource for instrument benchmarking and exploratory research. *Journal of sleep research*, 23(6):628–635, 2014.
- [42] Stanislas Chambon, Mathieu Galtier, Pierrick Arnal, Gilles Wainrib, and Alexandre Gramfort. A deep learning architecture for temporal sleep stage classification using multivariate and multimodal time series. *arXiv:1707.03321 [cs, q-bio, stat]*, November 2017. arXiv: 1707.03321.
- [43] Alexandre Gramfort, Martin Luessi, Eric Larson, Denis A. Engemann, Daniel Strohmeier, Christian Brodbeck, Roman Goj, Mainak Jas, Teon Brooks, Lauri Parkkonen, and Matti S. Hämäläinen. MEG and EEG data analysis with MNE-Python. *Frontiers in Neuroscience*, 7(267):1–13, 2013.
- [44] Robin Tibor Schirrmester, Jost Tobias Springenberg, Lukas Dominique Josef Fiederer, Martin Glasstetter, Katharina Eggersperger, Michael Tangermann, Frank Hutter, Wolfram Burgard, and Tonio Ball. Deep learning with convolutional neural networks for EEG decoding and visualization. *Human Brain Mapping*, aug 2017.
- [45] Takuya Akiba, Shotaro Sano, Toshihiko Yanase, Takeru Ohta, and Masanori Koyama. Optuna: A next-generation hyperparameter optimization framework. In *Proceedings of the 25rd ACM SIGKDD International Conference on Knowledge Discovery and Data Mining*, 2019.
- [46] Xi Wang and Junming Yin. Relaxed multivariate bernoulli distribution and its applications to deep generative models. In *Proceedings of the 36th Conference on Uncertainty in Artificial Intelligence (UAI)*, volume 124 of *Proceedings of Machine Learning Research*, pages 500–509. PMLR, 03–06 Aug 2020.

A Appendix

A.1 Details on EEG augmentations

Hereafter are some explanations concerning the implementation and continuous relaxation of each augmentation operation studied in this paper.

A.1.1 Frequency domain transforms

Frequency Shift To shift the frequencies in EEG signals, we carry a time domain modulation of the following form:

$$\text{FrequencyShift}(x)(t) := \text{Re}(\text{H}[x](t) \cdot \exp(2\pi i \Delta f t)), \quad (8)$$

where H denotes the Hilbert transform. At each call, a new shift Δf is sampled from a range linearly set by the magnitude μ , where $\mu = 1$ corresponds to the range $[0 - 5\text{Hz})$. This value was chosen after carrying data exploration, based on the observed shifts between subjects in the Physionet dataset.

Given that Equation 8 is completely differentiable on Δf , we only had to relax the sampling (using the pathwise derivatives trick [40]) to make it differentiable w.r.t μ . More precisely, we define $\Delta f = f_{\max} \cdot u$, where $f_{\max} = 5\mu$ is the frequencies range upper-bound and u is sampled from a uniform distribution over $[0, 1)$.

FT Surrogate In this transform, we compute the Fourier transform of the signal $\mathcal{F}(x)$ (using `fft`) and shift its phase using a random number $\Delta\varphi$:

$$\mathcal{F}(\text{FTSurrogate}(x))[f] := \mathcal{F}(x)[f] \cdot \exp(2\pi i \Delta\varphi).$$

We then transform it back to the time domain. This was reproduced from the authors [22] original code.¹ However, in our implementation we added a magnitude parameter setting the range in which random phases are sampled $[0, \varphi_{\max})$, with $\varphi_{\max} = 2\pi$ when $\mu = 1$.

The procedure used to make this transform differentiable is very similar to `frequency shift`,² with $\Delta\varphi$ parametrized as $\varphi_{\max}u$ and $\varphi_{\max} = 2\pi\mu$.

Bandstop Filter This transform was implemented using the FIR notch filter from MNE-Python package [43] with default parameters. The center of the band filtered out is uniformly sampled between 0 Hz and the Nyquist frequency of the signal. Here, the magnitude μ is used to set the size of the band, with $\mu = 1$ corresponding to 2 Hz. This value was chosen after some small experiments, where we observed that larger bands degraded systematically the predictive performance on Physionet.

This transformation was not relaxed (and hence not available to the gradient-based automatic data augmentation searchers).

A.1.2 Temporal domain transforms

White Noise This transform adds white Gaussian noise with a standard deviation set by the magnitude μ . When $\mu = 1$, the corresponding standard deviation was 0.2. Larger standard deviations would degrade systematically the predictive performance in our manual exploration on Physionet. The `white noise` implementation is straight forward. It's relaxation only included the use of pathwise derivatives for the sampling part: we sample the noise from a unit normal distribution and multiply it by the standard deviation $\sigma = 0.2 * \mu$.

Time Masking In this operation, we sample a central masking time t_{cut} with uniform probability (shared by all channels) and *smoothly* set to zero a window between $t_{\text{cut}} \pm \Delta t/2$, where Δt is the masking length. The latter is set by the magnitude μ , where $\mu = 1$ corresponds to $\Delta t = 1\text{s}$. This value was chosen because it corresponds roughly to the length of important sleep-related events.

The sampling part of the operation was made differentiable as above. Masking was computed by multiplying the signal by a function valued in $[0, 1]$, built with two opposing *steep* sigmoid functions

$$\sigma^\pm(t) = \frac{1}{1 + \exp(-\lambda(t - t_{\text{cut}} \pm \frac{\Delta t}{2}))},$$

¹<https://github.com/cliffordlab/sleep-convolutions-tf>

²It requires using Pytorch version 1.8, which now supports `fft` differentiation.

where λ was arbitrarily set to 1000.

A.1.3 Spatial domain transforms

Rotations

In this transform, we use standard sensors positions from a 10-20 montage (using the `mne.channels.make_standard_montage` function from MNE-Python package [43]). The latter are multiplied by a rotation matrix whose angle is uniformly sampled between $\pm\psi_{\max}$. The value of the maximum angle ψ_{\max} is determined by the magnitude μ , where $\mu = 1$ corresponds to $\frac{\pi}{6}$ radian (value used in [19, 23]). Signals corresponding to each channel are then interpolated towards the rotated sensors positions. While [19, 23] used radial basis functions to carry the interpolation, we obtained better results using a spherical interpolation, which also made more sense in our opinion.

The only part that needed to be relaxed to allow automatic differentiation was the rotation angle sampling, which was done as before, with the angle $\Delta\psi$ parametrized as $\psi_{\max}(2u - 1)$, u a uniform random variable in $[0, 1]$ and $\psi_{\max} = \frac{\pi}{6}\mu$.

Channel Dropout

Here, each channel is multiplied by a random variable sampled from a relaxed Bernoulli distribution [39, 46] with probability $1 - \mu$, where μ is the magnitude. This allows to set the channel to 0 with probability μ and to have a differentiable transform.

Channel Shuffle

In this operation, channels to be permuted are selected using relaxed Bernoulli variables as in the `channel_dropout`, but with probability μ instead of $1 - \mu$. The selected channels are then randomly permuted. As the permutation operation necessarily uses the channels indices, it is not straightforward to differentiate it, which is why we used a straight-through estimator here to allow gradients to flow from the loss to the magnitude parameter μ .

A.2 Magnitudes fine-tuning

In this section we explain the fine-tuning of magnitudes used for the manual exploration results presented in Section 5.

A first training with probability $p = 0.5$ and magnitude $\mu = 0.5$ was carried over the same training subsets as in Figure 3 and Figure 4. Then we selected the subset where the effects of augmentation were maximized (2^{-11} times the original training set for both Physionet and MASS datasets). Finally, for each operation, we carried a grid-search over the magnitude parameter (with fixed probability $p = 0.5$) with the selected training subsets (over 5-folds, as described in Section 5). The result of the grid-search can be seen on Figure A.1 and Figure A.2.

A.3 Further explanation concerning Straight Through magnitude gradient estimator

In order to validate the continuous relaxation of each augmentation operation described in Section A.1, we tried to *fit* the identity, *i.e.*, we minimized the mean squared error between augmented and unchanged batches of EEG signals:

$$\min_{p, \mu} \|X - \mathcal{O}(X; p, \mu)\|^2.$$

This allowed us to realize that using a simple straight-through estimator as suggested by [14] was not enough to learn good magnitude parameters. Indeed, we observed with many different learning rates that μ would be modified but would not converge to 0 when p was fixed. This motivated us to propose our own relaxation described in Section 4.2 and Section A.1.

A.4 Complementary results on EEG sleep data

A more complete version of figures Figure 5 and Figure 6 are Figure A.3 (where the time axis was not cropped) and Figure A.4 (where all operations are depicted). Each point in Figure A.3 corresponds to a moment where the search was stopped and the learned policy up to that point was used to retrain

the model from scratch and evaluate its final performance on the test set. For gradient-based methods (*i.e.*, (C)ADDA and Faster AutoAugment), we stop the search for evaluation every 5 epochs, while for gradient-free methods (Fast AutoAugment, standard and class-wise random search) we do it every 10 trials.

A.5 Limitations and future work

This work presents very promising results for sleep stage classification and would deserve more exploration beyond this application (*e.g.*, BCI, seizure detection).

A.6 Implementation

One will find included in this supplementary material the complete code of the MNIST experiment (Section 4.1). The code corresponding to the EEG experiments depends on many branches of existing projects, in particular `braindecode`³ which is still under heavy development. As it is quite difficult to package into a zip file, and its unlikely that reviewer would have time to run the experiments (which took weeks of GPU/hours computation on a HPC), we do not provide it in the supplementary. However, it will be made publicly available upon publication, and we plan on releasing a package compatible with `braindecode` and `PyTorch`.

³available <https://github.com/braindecode/braindecode>

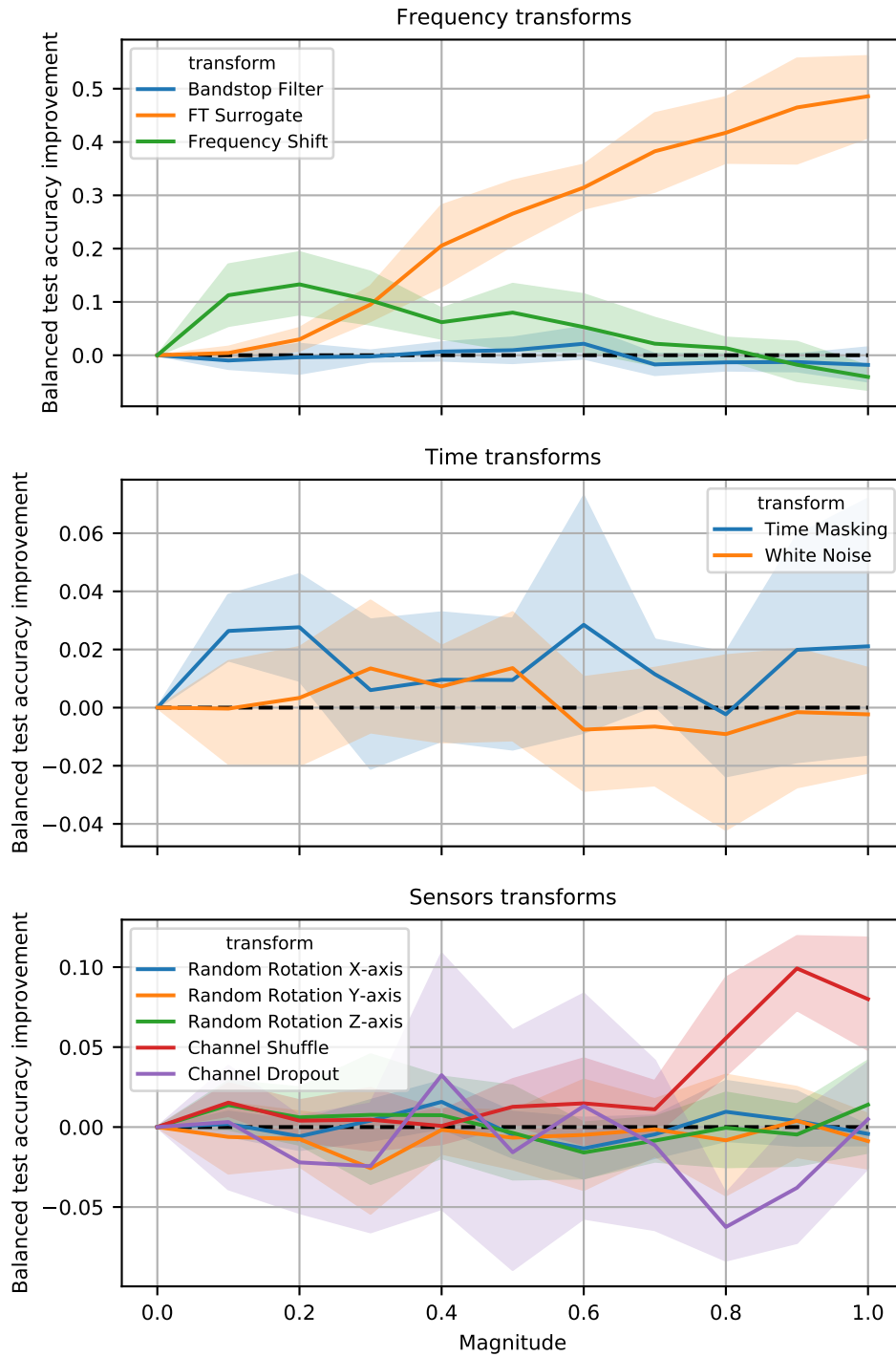


Figure A.1: Magnitudes grid-search results for Physionet dataset. Balanced accuracy values are relative to a training without any augmentation.

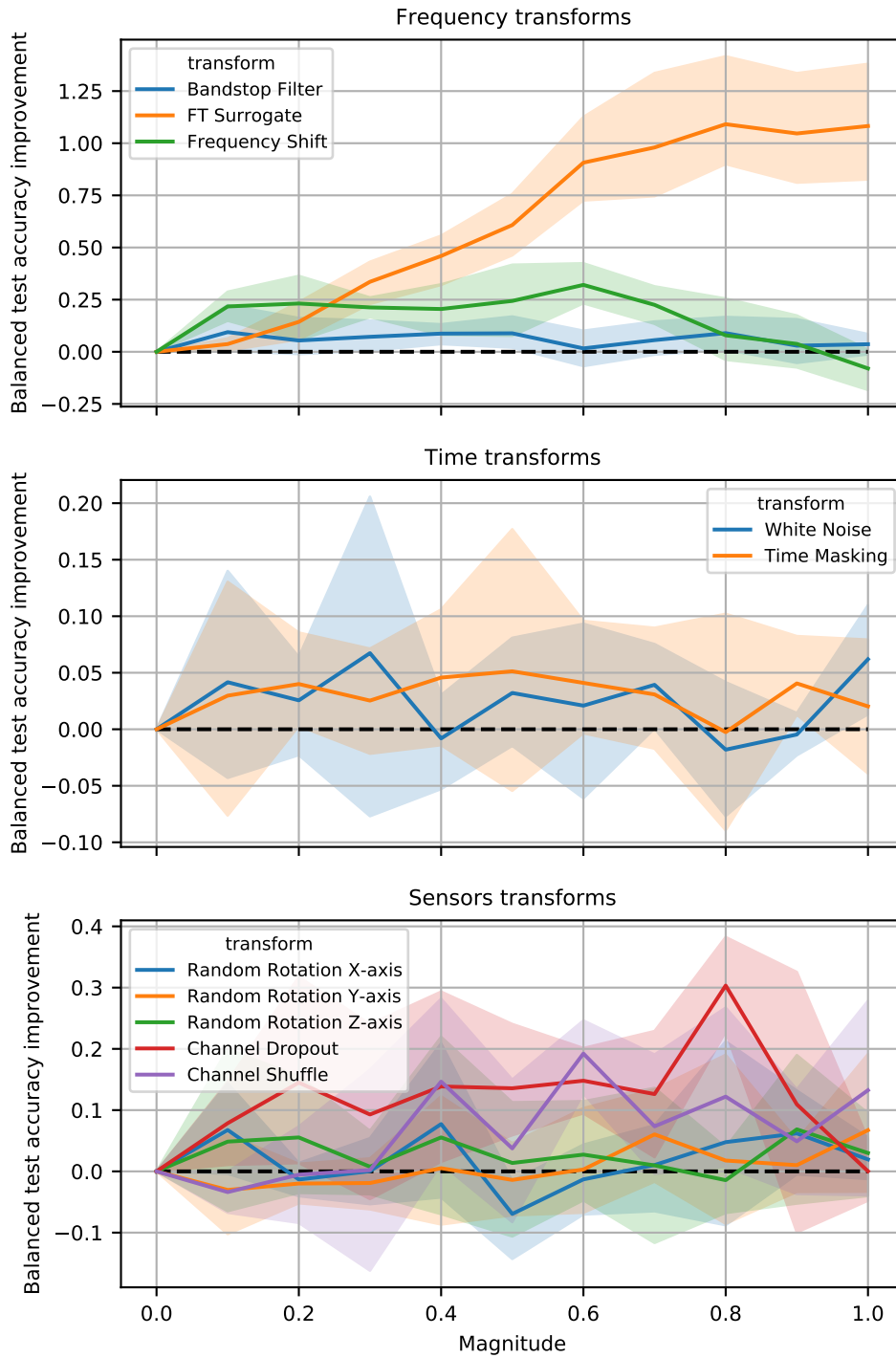


Figure A.2: Magnitudes grid-search results for MASS dataset. Balanced accuracy values are relative to a training without any augmentation.

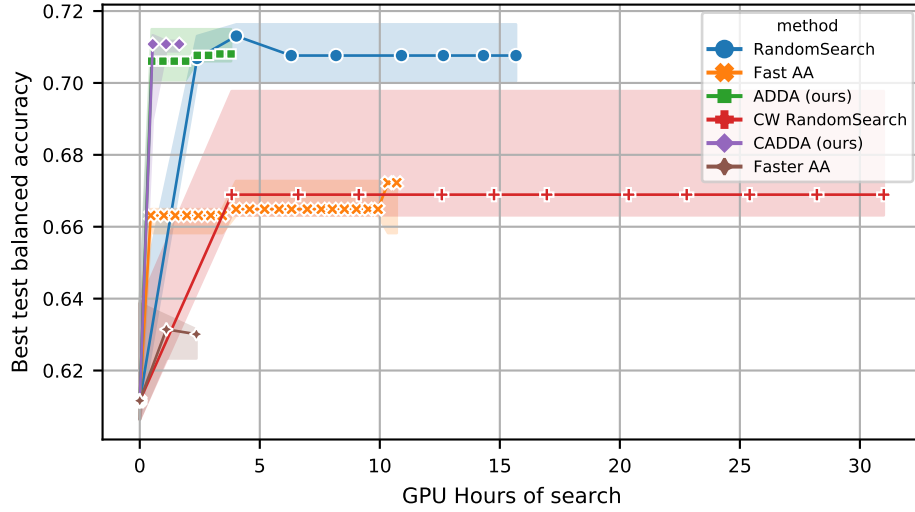


Figure A.3: Median performance obtained by different automatic data augmentation strategies as a function of the computation time.

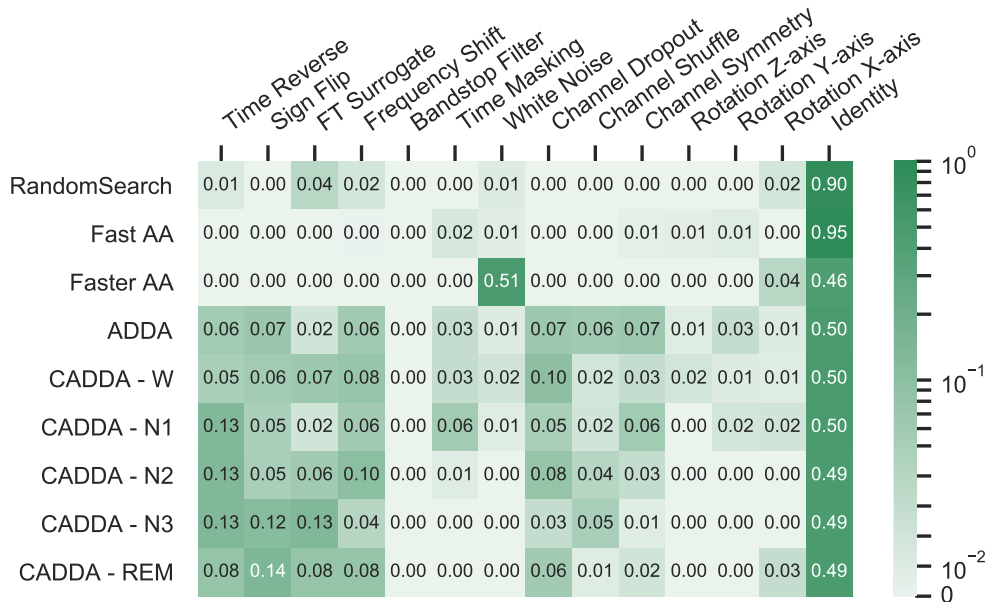


Figure A.4: Probability of applying each operation in the best policies obtained by the different search strategies. For each method, probabilities of all subpolicies are grouped.